SOFT ROBOTS

Soft wall-climbing robots

Guoying Gu[1,2*†], Jiang Zou[1*], Ruike Zhao[3,4], Xuanhe Zhao[3,5†], Xiangyang Zhu[1,2†]

Existing robots capable of climbing walls mostly rely on rigid actuators such as electric motors, but soft wall-climbing robots based on muscle-like actuators have not yet been achieved. Here, we report a tethered soft robot capable of climbing walls made of wood, paper, and glass at 90° with a speed of up to 0.75 body length per second and multimodal locomotion, including climbing, crawling, and turning. This soft wall-climbing robot is enabled by (i) dielectric-elastomer artificial muscles that generate fast periodic deformation of the soft robotic body, (ii) electroadhesive feet that give spatiotemporally controlled adhesion of different parts of the robot on the wall, and (iii) a control strategy that synchronizes the body deformation and feet electroadhesion for stable climbing. We further demonstrate that our soft robot could carry a camera to take videos in a vertical tunnel, change its body height to navigate through a confined space, and follow a labyrinth-like planar trajectory. Our soft robot mimicked the vertical climbing capability and the agile adaptive motions exhibited by soft organisms.

INTRODUCTION

Achieving the ability to climb walls with agile motions has long been a challenge in the field of robotics (*1*–*3*). Although a number of rigid wall-climbing robots have been developed with good performances in applications such as inspection, surveillance, and cleaning (*4*–*28*), they generally rely on complicated mechanisms composed of rigid actuators (such as electromagnetic or electrostatic motors) and transmission components (such as pulleys, wheels, or belts). As a result, these robots are usually heavy, and their bodies are inflexible, unlike animals. Soft wall-climbing robots based on muscle-like actuators in flexible bodies may have advantages—such as higher flexibility, better adaptability, and simpler design (*29*–*31*)—over their rigid counterparts.

Although soft robots capable of crawling (*32*–*35*), grabbing objects (*36*, *37*), camouflaging (*38*, *39*), swimming (*40*–*42*), and growing (*43*) have recently been developed with pneumatic actuators, shape memory alloys, or dielectric-elastomer actuators, soft wall-climbing robots have not yet been achieved. A recent work reported a tethered soft robot based on pneumatic actuators that could crawl inside a vertical tube (*44*), but it still could not climb flat walls. The challenges for developing soft wall-climbing robots include (i) the design and integration of soft actuators and adhesive components in a flexible robotic structure and (ii) the control of the actuators and adhesive components in a synchronized manner to achieve swift and stable climbing.

Here, we present a tethered soft robot that can climb various walls at 90°, carry a payload, and exhibit multimodal locomotion capability. We achieved the soft wall-climbing robot by developing and integrating (i) a dielectric-elastomer actuator that generated fast periodic deformation of the soft robotic body (Fig. 1A), (ii) two electroadhesive feet with separate spatiotemporally controlled adhesion on walls (Fig. 1B), and (iii) a control strategy that synchronized the body deformation and feet adhesion for stable climbing (Fig. 1C). A finite element model was also developed to aid the design of the dielectric-elastomer actuator to achieve different climbing modes. We demonstrate that our tethered soft robot could climb various walls made of wood, paper, and glass at 90° with 0.75 body length per second (63.43 mm/s; movie S1), crawl on horizontal planes with a speed of 1.04 body lengths per second (88.46 mm/s; movie S3), and achieve spot-turning locomotion with a speed of 62.79° per second (movie S4). The soft robot could also carry a payload while climbing vertical walls (movie S2). By carrying a camera, our soft robot could record videos while climbing in a narrow vertical tunnel (movie S5). We further show that it successfully navigated through a low corridor that was 58.33% shorter than its body height (movie S6) and tracked a complex planar labyrinth-like trajectory (movie S7).

RESULTS

Design and operation principles of the soft wall-climbing robot

Figure 1 shows the components of the soft wall-climbing robot and its operation principle. The soft robot comprises a dielectric-elastomer actuator as its deformable body and two double-pole electroadhesive pads as its feet with controlled adhesion (details on fabrication and assembly of the soft robot can be found in figs. S1 to S3). The dielectric-elastomer actuator consists of a prestretched dielectric-elastomer membrane and a flexible acrylic frame (Fig. 1A). The dielectric-elastomer membrane (VHB 4910; undeformed thickness, 1 mm) was biaxially prestretched five times, sandwiched by two compliant carbon grease electrodes (Fig. 1A, left), and adhered on the acrylic frame (thickness, 0.3 mm). After relaxing the prestretched membrane, the dielectric-elastomer actuator buckled to a saddle-shaped structure (Fig. 1A, middle) (*45*). As the applied voltage on the dielectric-elastomer actuator (V_A) increased or decreased, the body of the soft robot extended or contracted (*46*–*48*), respectively. In the Supplementary Materials, we provide a simulation model to predict the deformation of the dielectric-elastomer actuator, and the simulation results (fig. S4) showed good agreement with the experiments.

The deformation of the dielectric-elastomer actuator resulted in symmetric movements of both feet due to the same friction between the feet and the substrate (*32*–*34*), which could not move the robot forward. To address this, we next designed the electroadhesive feet for the soft robot and investigated their effect on climbing walls. Our

[1]Robotics Institute, School of Mechanical Engineering, Shanghai Jiao Tong University, Shanghai 200240, China. [2]State Key Laboratory of Mechanical System and Vibration, Shanghai Jiao Tong University, Shanghai 200240, China. [3]Soft Active Materials Laboratory, Department of Mechanical Engineering, Massachusetts Institute of Technology, Cambridge, MA 02139, USA. [4]Department of Mechanical and Aerospace Engineering, Ohio State University, Columbus, OH 43210, USA. [5]Department of Civil and Environmental Engineering, Massachusetts Institute of Technology, Cambridge, MA 02139, USA.
*These authors contributed equally to this work.
†Corresponding author. Email: guguoying@sjtu.edu.cn (G.G.); zhaox@mit.edu (X. Zhao); mexyzhu@sjtu.edu.cn (X. Zhu)

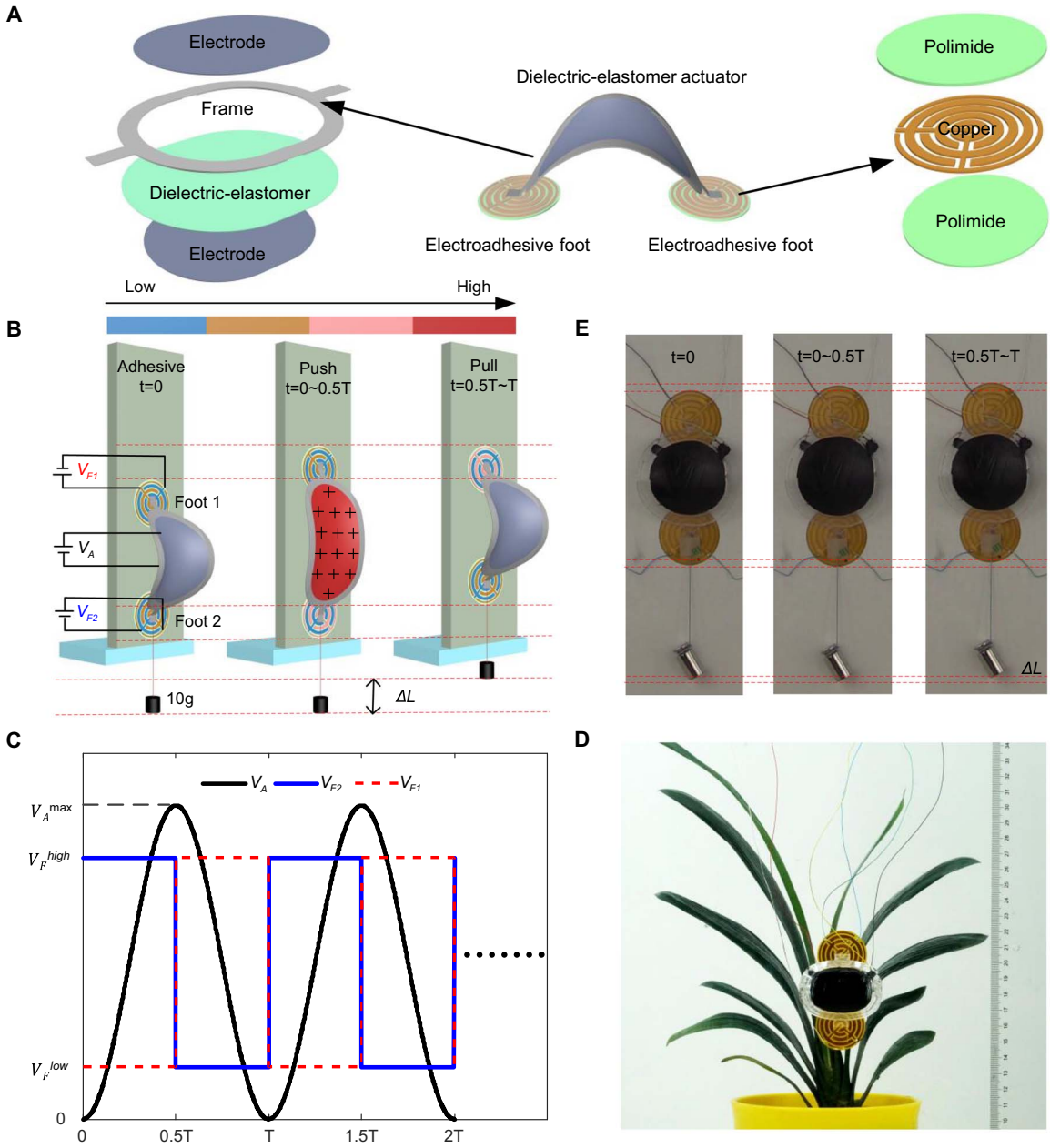

Fig. 1. Design and operation principles of the soft wall-climbing robot. (**A**) The soft robot integrates a dielectric-elastomer actuator as its deformable body and two double-pole electroadhesive pads as its feet, with controlled adhesion. (Left) The actuator consists of a biaxially prestretched (five times) dielectric-elastomer membrane (VHB 4910; undeformed thickness, 1 mm), sandwiched by two compliant electrodes (carbon grease), and a flexible frame (thickness, 0.3 mm). (Middle) After relaxing the prestretched membrane, the actuator buckles to a saddle-shaped structure. (Right) Each electroadhesive foot consists of a copper electrode layer (thickness, 0.018 mm) sandwiched by two polyimide layers (thickness of each layer, 0.02 mm). (**B**) Schematic of the climbing principle. The dielectric-elastomer actuator (sinusoidal voltage V_A with period T) extends or contracts while switching the applied square voltage to two electroadhesive feet. Over each cycle, the soft robot climbs up by a distance of ΔL. (**C**) Sequence of the control voltages for the actuator and electroadhesive feet to achieve the climbing locomotion. (**D**) Still image of climbing upon a transparent glass wall (movie S1). (**E**) Still images of the climbing process with a 10-g payload on the wood I wall (movie S2).

electroadhesive foot consists of an electrode layer (copper; thickness, 0.018 mm) sandwiched by two polyimide layers (thickness, 0.02 mm), where the top polyimide insulated the electrode layer from outside and the bottom polyimide worked as a dielectric layer for adhesion on walls (Fig. 1A, right). The electroadhesive foot was fabricated with the interdigitated concentric electrode (diameter, 32 mm; see fig. S1) for its superior electroadhesive performance (*49*, *50*). When a voltage V was applied to either electroadhesive foot (V_{F1} or V_{F2}), the corresponding foot could adhere to the wall.

Climbing on walls further requires a synergy between the deformation of the robotic body (controlled by V_A) and the adhesion of both feet (controlled by V_{F1} and V_{F2}) (Fig. 1B). We developed a control

strategy to synchronize these applied voltages to achieve stable climbing on walls. Figure 1C shows the sequence of V_A and V_{F1} and V_{F2} within a repeated period of time, T. Each cycle of climbing locomotion involved two steps. At the first step (t = 0 to ~0.5 T), the voltage applied to the front foot, V_{F1}, was a relatively low value, V_F^{low}, and that on the rear foot V_{F2} was a relatively high value, V_F^{high}; thus, the tangential force required to slide the front foot was smaller than that of the rear foot. With V_A increasing from zero to its maximum value, V_A^{max}, following a sinusoidal function, the actuator extended and pushed the front foot to move up (Fig. 1B, middle). At the second step (t = 0.5 to ~1 T), the voltages V_{F1} and V_{F2} were switched to V_F^{high} and V_F^{low}, respectively, so that the tangential force for sliding the rear foot was lower. With V_A decreasing from its maximum value V_A^{max} to zero, the actuator contracted and lifted up the rear foot together with the payload (Fig. 1B, right).

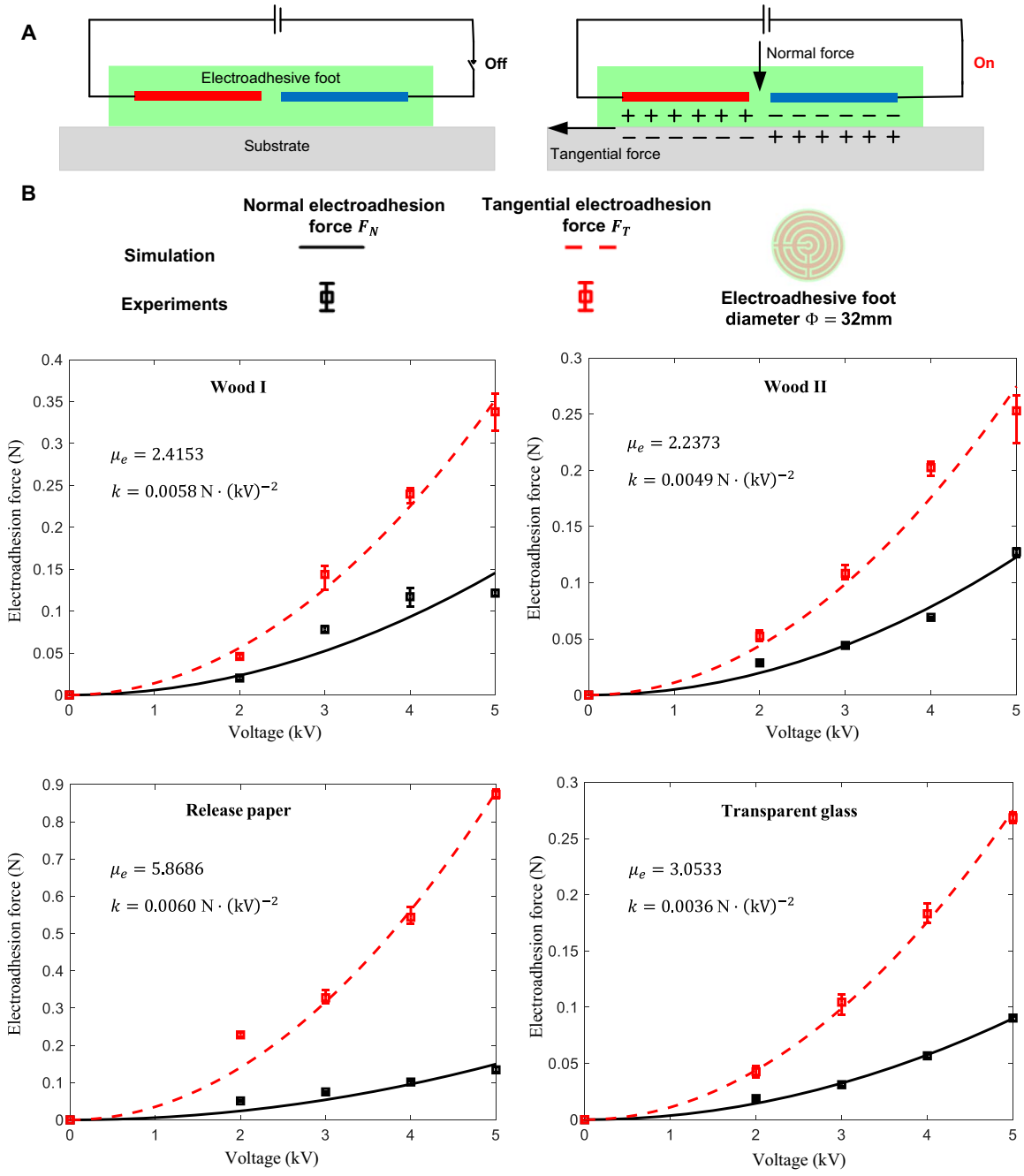

Fig. 2. Characterization of the electroadhesion forces of the foot. (**A**) Schematic description of the electroadhesion: When a voltage is applied across the electrode, opposite net charges are polarized in the area of the foot, producing the electroadhesion forces between the foot and the substrate in the normal and tangential directions. (**B**) F_N and F_T are plotted as functions of V_F on four substrates, including wood I, wood II, release paper, and transparent glass. Black and red markers represent measured values of the normal and tangential electroadhesion forces, respectively. Black solid and red dashed lines represent predictions from Eqs. 1 and 2, respectively. Error bars indicate the SD for n = 5 measurements at each data point.

Thereafter, the patterns of applied voltages on the actuator and electroadhesive feet were repeated at the frequency of $1/T$. Over each cycle, the soft robot climbed up by an extension length, ΔL (Fig. 1B). Therefore, the climbing speed of the soft robot can be calculated by $\Delta L/T$. Figure 1D and movie S1 demonstrate that the soft robot climbed a transparent glass wall at 90°. Figure 1E and movie S2 further show that the soft robot climbed a wood wall at 90° while carrying a 10-g payload.

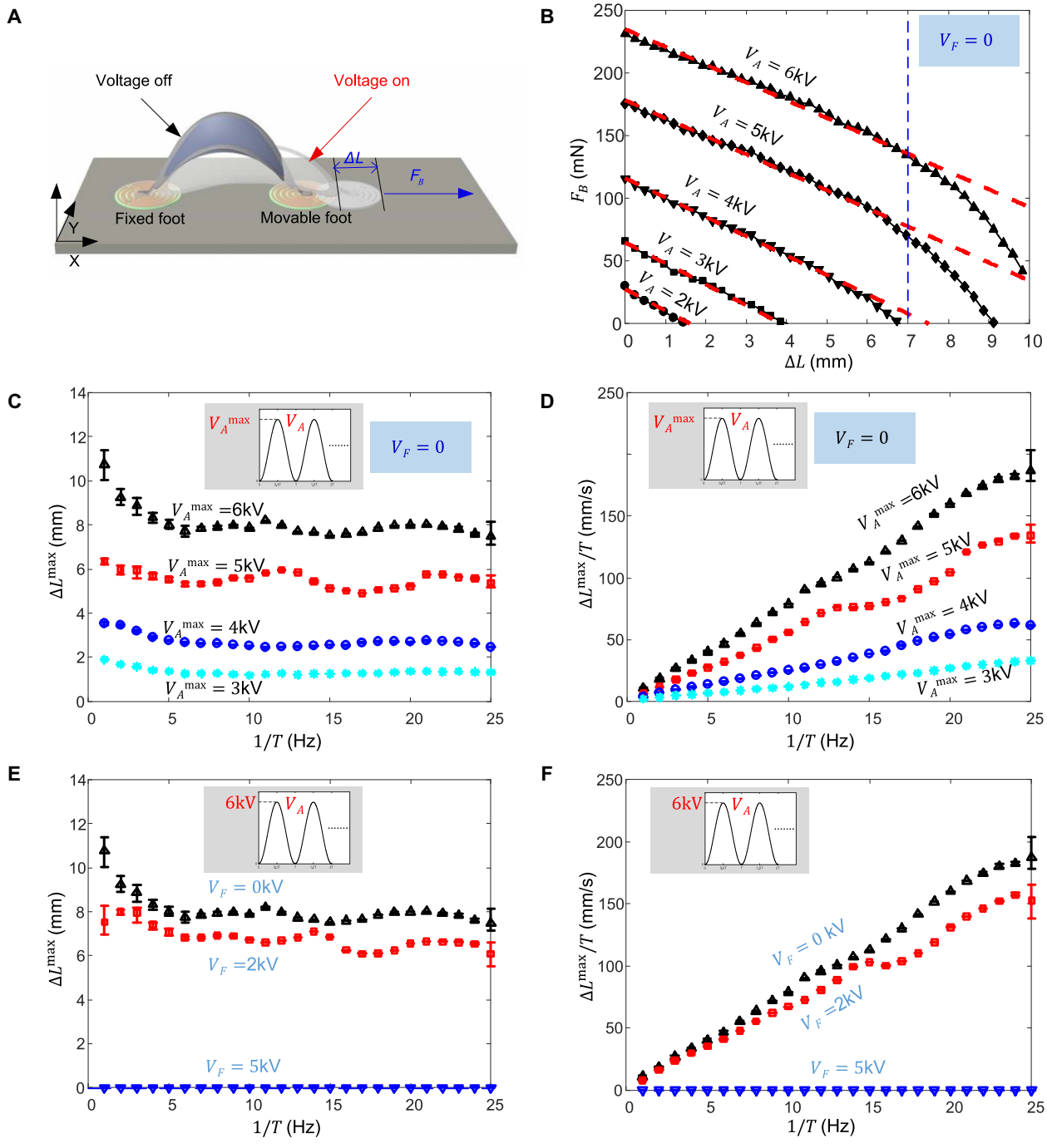

Fig. 3. Characterization of the blocking force and extension length of the actuator. (**A**) Schematic description of F_B and ΔL generated by the actuator. Throughout the measurements, we fixed one foot on the substrate and measured ΔL and F_B of the other movable foot by applying voltages on the dielectric-elastomer actuator and the movable foot. (**B**) F_B is plotted as a function of ΔL under step voltages on the actuator V_A (i.e., DC voltages: 2, 3, 4, 5, and 6 kV). Markers represent measured values, and dashed lines represent linear fitting. (**C**) ΔL^{max} is plotted as a function of $1/T$ under sinusoidal voltages V_A (i.e., AC voltages) with various maximum voltages on the actuator V_A^{max} (i.e., 3, 4, 5, and 6 kV) and zero voltage on the movable foot (i.e., $V_F = 0$). (**D**) $\Delta L^{max}/T$ is plotted as a function of $1/T$ based on the measured ΔL^{max} in (C). (**E**) ΔL^{max} is plotted as a function of $1/T$ under the sinusoidal voltages V_A (i.e., AC voltages) with a constant maximum voltage on the actuator $V_A^{max} = 6$ kV and different values of V_F (i.e., DC voltages: 0, 2, and 5 kV). (**F**) $\Delta L^{max}/T$ of the movable foot is plotted as a function of $1/T$ based on ΔL^{max} in (E). Error bars indicate the SD for $n = 5$ measurements at each data point.

Characterization of the electroadhesive feet

We integrated a dielectric-elastomer actuator and two electroadhesive feet to constitute a soft robot and proposed a controllable locomotion mechanism for the soft robot to climb walls. This method relies on the synergy of the electroadhesion between the feet and the substrate and the deformation of the dielectric-elastomer actuator. We first characterized the electroadhesion forces (F) as a function of the applied voltages on the feet and investigated how the applied voltages affected the electroadhesion forces when they moved on different substrates (such as wood, paper, and glass).

When a voltage was applied across the electrode on an electroadhesive foot, opposite net charges were polarized in the area of the foot because of the electrostatic effect (*49*, *50*). As a result, to move the foot on the substrate along the normal and tangential directions, certain normal and tangential forces, respectively, are required (Fig. 2A). These forces are named the normal and tangential electroadhesion forces of the foot on the substrate, respectively. Because electroadhesion mainly relies on the dielectric effect, the normal electroadhesion force scales with the square of the applied voltage (*50*, *51*):

$$F_N = kV_F^2 \quad (1)$$

where k is a dimensional constant $[N \cdot (kV)^{-2}]$ that depends on the geometries and materials of the electrode and substrates. The tangential electroadhesion force can be expressed as

$$F_T = \mu_e F_N \quad (2)$$

where μ_e denotes the effective frictional coefficient of the interface between the foot and the substrate. To identify the coefficients k in Eq. 1 and μ_e in Eq. 2, we measured the forces required to pull an electroadhesive foot away from different substrates under various applied voltages along the normal and tangential directions, respectively (see fig. S5 for a detailed experimental description). Because the breakdown voltage (*51*, *52*) of the electroadhesive foot is ~6 kV, we applied four V_F values (i.e., 2, 3, 4, and 5 kV) in the tests. The measured normal and tangential electroadhesion forces are plotted in Fig. 2B. Equations 1 and 2 reasonably predicted the measured forces with fitted parameters of k = 0.0058, 0.0049, 0.0060, and 0.0036 $N \cdot (kV)^{-2}$ and μ_e = 2.4153, 2.2373, 5.8686, and 3.0533 for four substrates of wood I, wood II, release paper, and transparent glass, respectively. Notably, the experimental results demonstrate that F_T is larger than F_N, possibly due to the restriction force caused by the edge effect of the electrodes in the foot (*52*, *53*). The minor deviation of the experimental data from Eqs. 1 and 2 is likely due to the fact that the electrostatic adhesion is also affected by environmental parameters (e.g., humidity and temperature), nonuniform charge distribution on the interface, dielectric relaxation, and charge leakage (*49*, *52*).

Characterization of the dielectric-elastomer actuator

Next, we characterize the performance of the dielectric-elastomer actuator and investigate how the electroadhesion forces affect the ability of the actuator to move. Without the applied voltage, the dielectric-elastomer actuator has an initial length. Under V_A, the actuator can elongate by ΔL and generate a blocking force, F_B, which is defined as the required force to fix the actuator at a certain extension length under an applied voltage (see fig. S6 for the detailed experimental description). Both ΔL and F_B are critical to the design of a climbing robot because the robot needs to elongate and contract against sliding forces to climb walls. To characterize the force extension performance of the dielectric-elastomer actuator, we measured F_B as a function of ΔL under different V_A values (i.e., 2, 3, 4, 5, and 6 kV). Throughout the measurement, we fixed one foot on the substrate and measured ΔL and F_B of the other movable foot (Fig. 3A; see figs. S6 and S7 for detailed experimental description). In Fig. 3B, we show the F_B versus ΔL curves for various V_A values. F_B monotonically decreased with the increase of the extension length. When F_B was zero, ΔL reached its maximum, and when ΔL was zero, F_B reached its maximum. In addition, we found that a simple linear stiffness model approximately represented the relationship between F_B and ΔL up to ΔL = 7 mm (Fig. 3B).

We next applied a sinusoidal voltage on the actuator $V_A = V_A^{max}\left[\frac{1}{2}\sin(2\pi t/\ T - \pi/2) + \frac{1}{2}\right]$ and a constant voltage on the movable

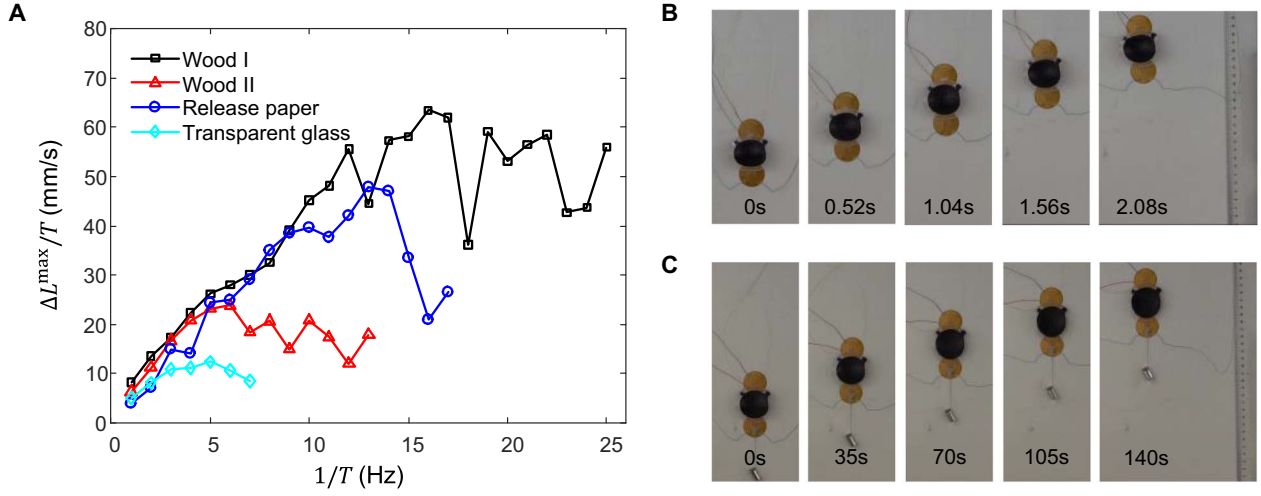

Fig. 4. Climbing results of the soft robot. (**A**) $\Delta L^{max}/T$ plotted as a function of $1/T$ on four substrates: wood I, wood II, release paper, and transparent glass (movie S1). The maximum climbing speed can reach 63.43 mm/s (0.75 body length per second) on the wood I wall. The speeds were averaged from at least 10 periods per frequency according to the recorded videos. (**B**) Still images illustrate the climbing process of the soft robot on the wood I wall. (**C**) Still images illustrate the climbing process of the soft robot with a 10-g payload (movie S2).

foot, V_F, and then measured the maximum extension length, ΔL^{max}, at each cycle achieved by the actuator (see figs. S7 and S8 for the detailed experimental description). At the quasi-static state, ΔL^{max} can be achieved when F_B under V_A^{max} is equal to F_T of the movable foot under V_F. Therefore, ΔL^{max} can be solved by

$$F_T(V_F) = F_B(V_A^{max}, \Delta L^{max}) \quad (3)$$

In Fig. 3C, we plotted ΔL^{max} as a function of $1/T$ under various maximum voltages on the actuator V_A^{max} (i.e., 3, 4, 5, and 6 kV) and zero voltage on the movable foot ($V_F = 0$). We obtained the predicted ΔL^{max} under quasi-static conditions by solving Eq. 3 with $V_F = 0$ and various values of V_A^{max}. When $1/T$ of the sinusoidal voltage on actuator was low, ΔL^{max} predicted by Eq. 3 consistently matched with the measured values. As the frequency increased, ΔL^{max} tended to decrease, possibly due to dynamics of the actuator. In Fig. 3D, we plotted the moving speed, $\Delta L^{max}/T$, of the movable foot as a function of $1/T$ of V_A. Overall, $\Delta L^{max}/T$ increased with the increase of the frequency.

Next, we fixed V_A^{max} to be 6 kV and varied V_F on the movable foot (i.e., 0, 2, and 5 kV) to measure ΔL^{max}. In Fig. 3E, we plotted the measured ΔL^{max} as a function of $1/T$ for various V_F values on the movable foot. With the increase of V_F on the movable foot, ΔL^{max} in the quasi-static condition decreased, which also consistently

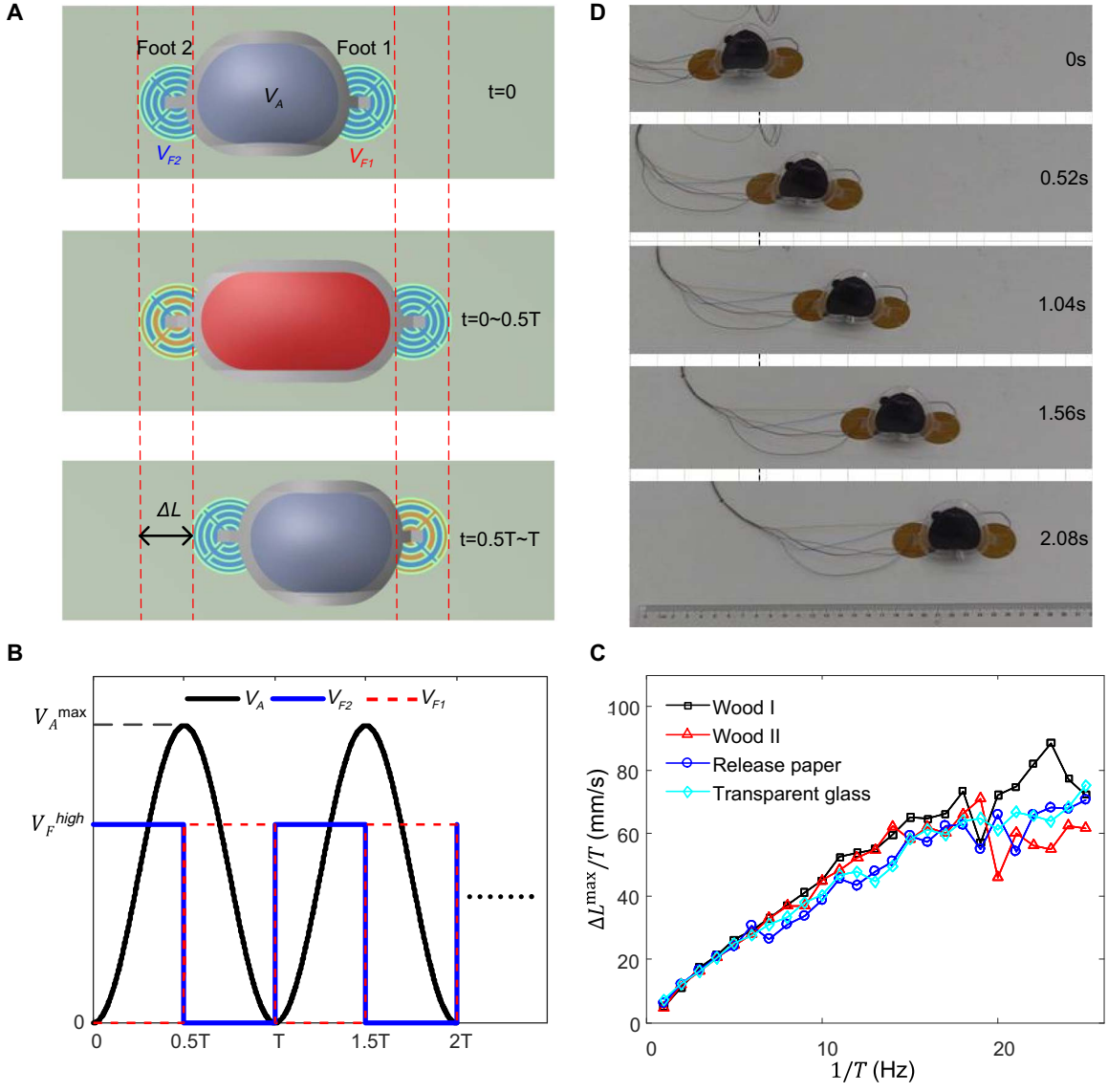

Fig. 5. Crawling results of the soft robot. See also movie S3. (**A**) Schematic description of the crawling principle of the soft robot on a horizontal plane: Driving the dielectric-elastomer actuator (sinusoidal voltage V_A with period T) to extend or contract while switching the applied square voltage to the electroadhesive feet. Over each cycle, the soft robot crawls by a distance of ΔL. (**B**) Sequence of the control voltages for the dielectric-elastomer actuator (V_A) and the electroadhesive feet (V_{F1} and V_{F2}) to achieve the crawling locomotion. (**C**) $\Delta L^{max}/T$ plotted as a function of $1/T$ on four substrates: wood I, wood II, release paper, and transparent glass. The maximum crawling speed can reach 88.46 mm/s (1.04 body lengths per second) on the wood I plane. The speeds were averaged from at least 10 periods per frequency according to the recorded videos. (**D**) Still images illustrate the crawling process on the wood I plane.

matched with the measured ΔL^{max} at low frequencies of the voltage on the actuator (Fig. 3E). As $1/T$ increased, ΔL^{max} for each V_F also decreased, possibly due to dynamics of the robot (*48*, *52*). Notably, if $F_T > F_B$ when $\Delta L^{max} = 0$, then both the model and experimental measurements showed that the foot could not move on the substrate at all (e.g., the case of $V_A^{max} = 6$ kV and $V_F = 5$ kV in Fig. 3E). In addition, from Fig. 3F, we see that $\Delta L^{max}/T$ increased with the increase of the frequency for various V_F values.

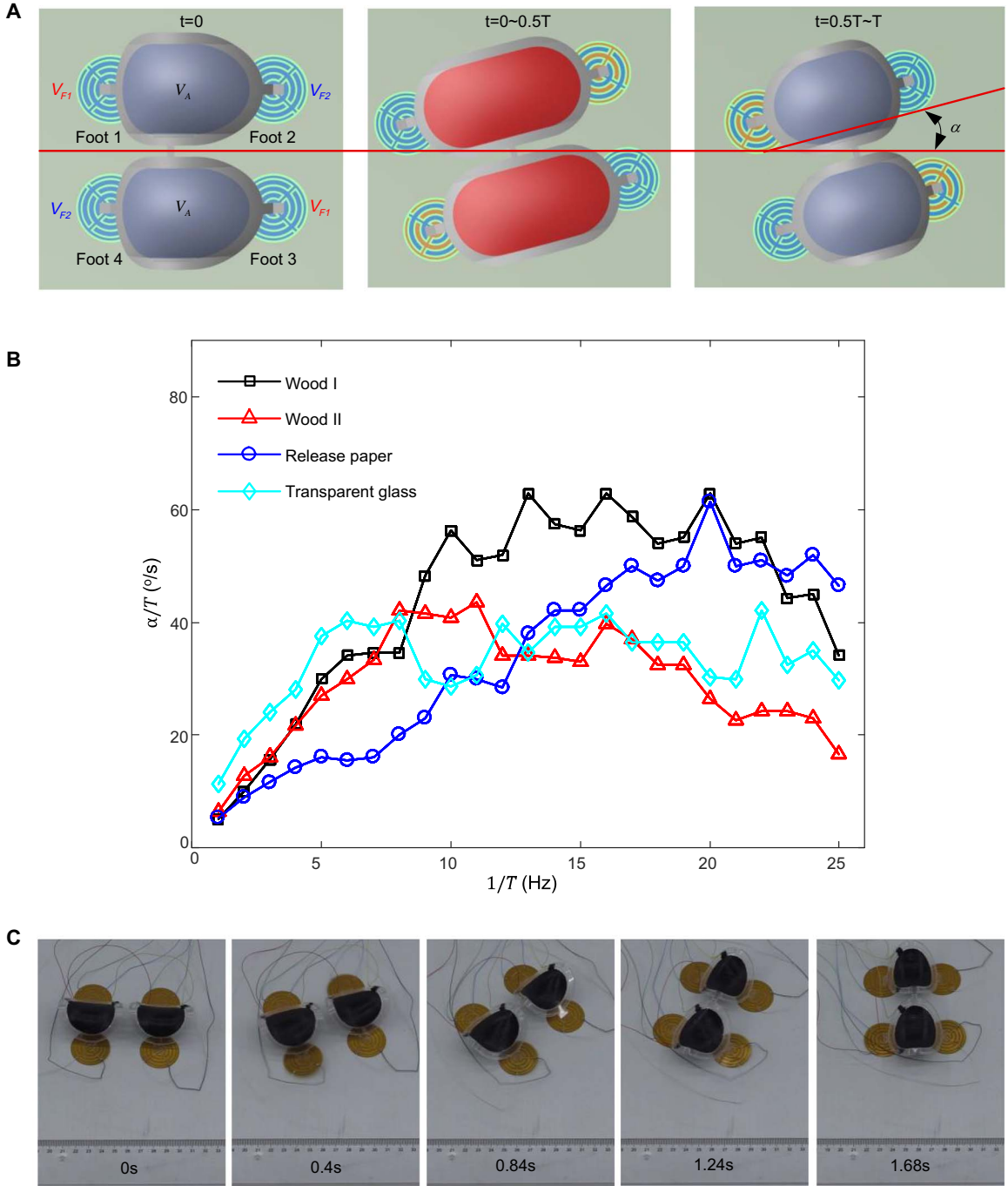

Fig. 6. Turning results of the soft robot. See also movie S4. (**A**) Schematic description of the spot turning principle of a four-feet soft robot on the horizontal plane, driving the two dielectric-elastomer actuators (sinusoidal voltage V_A, with the period of T) to extend or contract while switching the applied square voltage to the electroadhesive feet (V_{F1} for feet 1 and 3 and V_{F2} for feet 2 and 4, with the period of T). Over each cycle, the soft robot turns by an angle of α. The sequence of control voltages for the dielectric-elastomer actuators (V_A) and electroadhesive feet (V_{F1} and V_{F2}) to achieve the turning locomotion was the same as in Fig. 5B. (**B**) The turning speed α/T (degree per second) is plotted as a function of $1/T$ on four substrates: wood I, wood II, release paper, and transparent glass. The maximum turning speed is 62.79° per second on the wood I plane. The speeds were averaged from at least 10 periods per frequency according to the recorded videos. (**C**) Still images illustrate the spot turning process on the wood I plane.

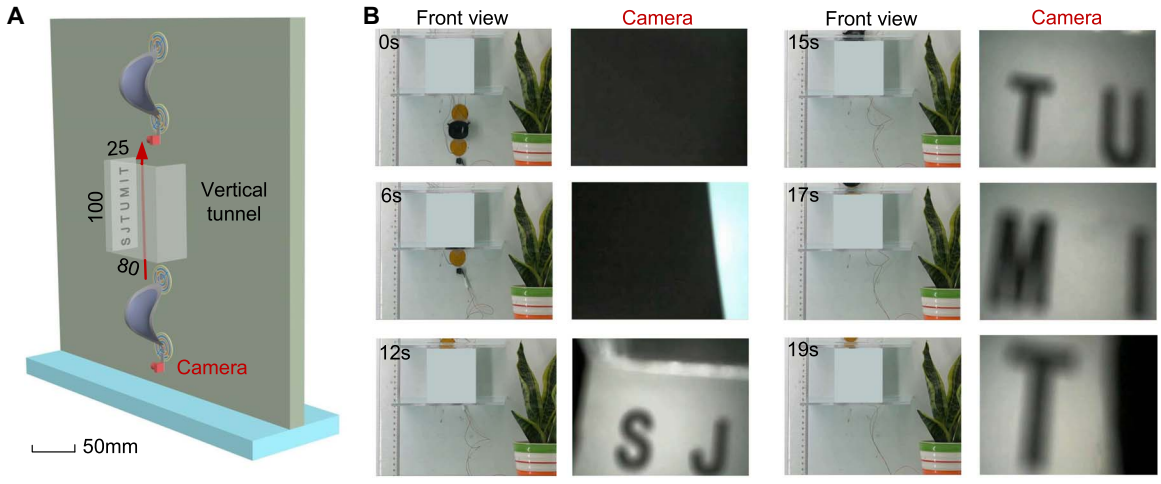

Fig. 7. Demonstration of the video recording function in a confined vertical tunnel. See also movie S5. The soft wall-climbing robot takes videos while climbing up a vertical tunnel (length, 100 mm; width, 80 mm; height, 25 mm) to record letters "S," "J," "T," "U," "M," "I," and "T" printed on the wall of the tunnel. (**A**) Schematic illustration of the function. (**B**) Still images of the wall-climbing and video recording process of the robot.

Climbing results

For stable climbing, the foot under V_F^{high} should provide a F_T that is higher than the maximum F_B generated by the actuator to avoid sliding or detaching of the robot,

$$F_T(V_F^{high}) > F_B(V_A^{max}, \Delta L = 0) \quad (4)$$

The deformation of the dielectric-elastomer actuator pushes or pulls the other foot under V_F^{low} to climb up (Fig. 1B). During climbing, ΔL^{max} of the robot in the quasi-static condition can be calculated by solving Eq. 3. To maximize $\Delta L^{max}/T$, the sinusoidal V_A^{max} should be as large as possible (Fig. 3D). However, a high applied voltage on the actuator (i.e., more than~6.5 kV) can induce the electromechanical instability of the dielectric elastomer (*45*–*48*). In the climbing experiments, we used the sinusoidal voltage on the actuator with V_A^{max} = 6 kV to avoid the electromechanical instability. In movie S1, we demonstrated agile climbing locomotion of our soft robot on four substrates, including wood I, wood II, release paper, and transparent glass, with different amounts of roughness (fig. S9). From Fig. 4A, it can be seen that $\Delta L^{max}/T$ became larger with the increase of the frequency but tended to decrease after a certain value of the frequency due to the dynamics of the robot. $\Delta L^{max}/T$ also relied on the materials and surface roughness of the substrate. Our soft robot climbed the wood I wall with the maximum speed of 63.43 mm/s (0.75 body length per second) at the frequency of 16 Hz (movie S1).

To demonstrate our soft robot's capability of carrying payloads, we attached an additional weight to the rear foot of the robot. Increasing the weight of the payload was expected to decrease the climbing speed. In Fig. 4C and movie S2, our soft robot climbed the wood I wall at a lower speed of 1 mm/s when a 10-g payload was attached.

Crawling and turning results

Next, we demonstrate that our soft wall-climbing robot could also crawl on horizontal planes (termed the crawling mode; Fig. 5). Figure 5B shows the sequence of V_A and V_{F1} and V_{F2} within a repeated T. In Fig. 5C, $\Delta L^{max}/T$ mostly increased with the frequency of applied voltages, but there were few exceptions to this trend. The maximum crawling speed of the robot was 88.46 mm/s (1.04 body lengths per second), which was achieved on the wood I substrate at the input frequency of 23 Hz (movie S3).

Whereas existing soft crawling robots (*32*–*34*) generally do not have the turning capability, our design of the two-foot soft robot can be scaled up to a four-foot soft robot to give the spot-turning locomotion (Fig. 6). In this turning mode, we divided the four feet into two groups, where feet 1 and 3 were in one group and feet 2 and 4 were in the other group (Fig. 6A). Following the sequence of voltages applied on four feet (V_{F1} for feet 1 and 3 and V_{F2} for feet 2 and 4) and two actuators (V_A) (Fig. 5B), the four-foot soft robot achieved the turning locomotion. In Fig. 6B, the turning speed α/T (α is the measured turning angle at each T as illustrated in Fig. 6A) on four substrates was plotted as a function of $1/T$. The results indicate that our soft robot turned on the wood I plane with the maximum speed of 62.79° per second at the input frequency of 20 Hz (movie S4).

Applications of our soft robots

We next demonstrate a few potential applications enabled by our soft robot's capabilities. For example, the capabilities of climbing in confined spaces and agile locomotion make the robot suitable for inspection and surveillance in special environments. We added a small camera (weight, 1 g; model-MC900, 3RDEE Co. Ltd.) on our robot, so that it could take videos while climbing a vertical confined tunnel (length, 100 mm; width, 80 mm; height, 25 mm). As a result, the soft robot recorded the letters "S," "J," "T," "U," "M," "I," and "T" printed on a side wall of the tunnel (Fig. 7 and movie S5).

New functions and applications also arise from our soft robot's flexibility and capabilities of crawling and turning. Figure 8A and movie S6 demonstrate that our soft robot deformed its body to successfully crawl through a low corridor (height, 10 mm; 41.67% of the robot's height without applied voltage), albeit at a slower speed than the normal one. In another application, we drove a four-foot soft robot through a complicated path with various turns (Fig. 8B and movie S7). Our soft robot successfully went through the labyrinth-like trajectory (total lengths of 1.8 m with two left turns and four right turns) within 50 s.

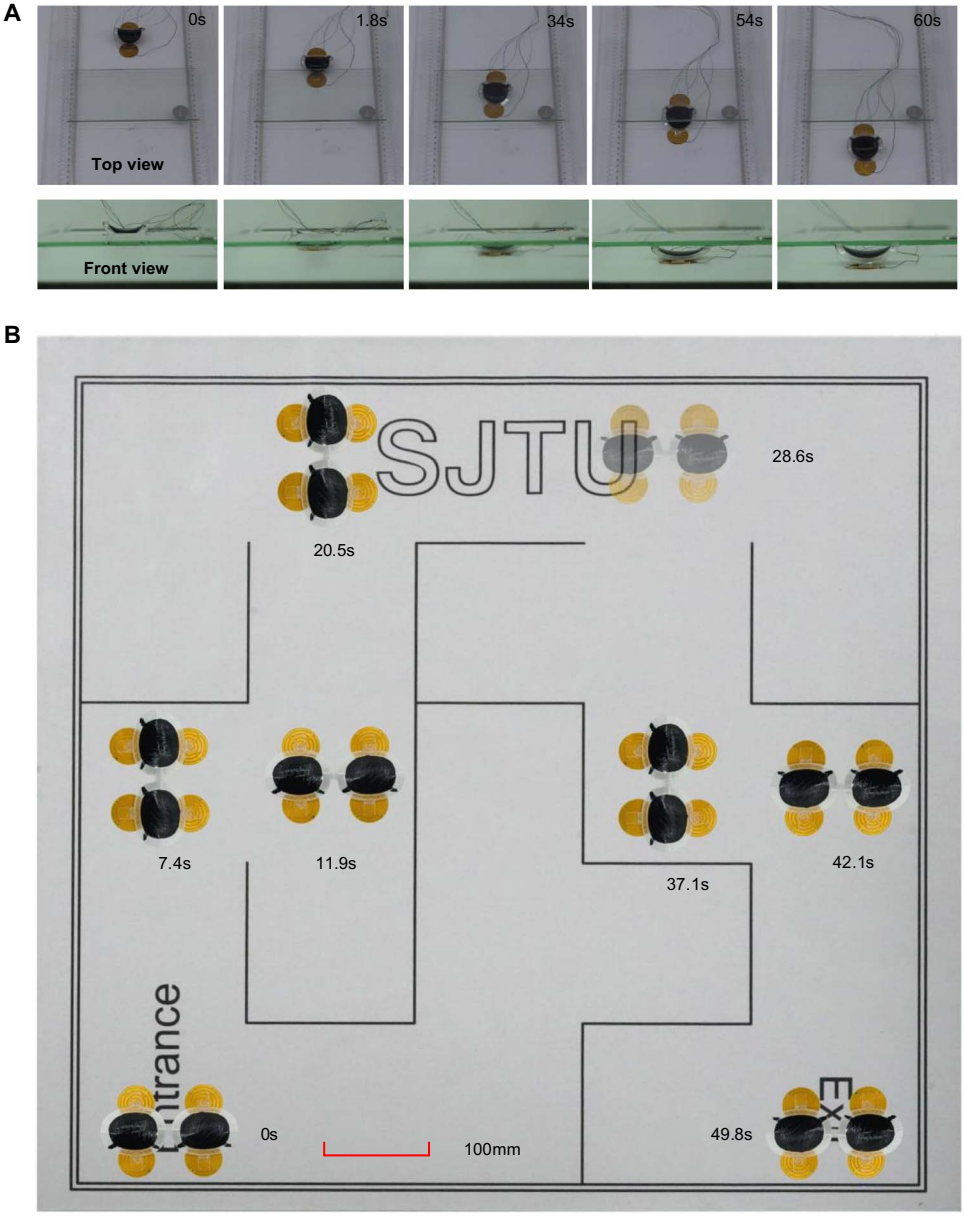

Fig. 8. Demonstration of confined space navigation and labyrinth trajectory tracking. (**A**) A two-foot soft robot navigates through the low corridor with the height of 10 mm (58.33% shorter than its body height, movie S6). (**B**) A four-foot soft robot tracks a planar labyrinth-like trajectory (total lengths of 1.8 m with two left-angled turnings and four right-angled turnings) within 50 s (movie S7).

DISCUSSION

In summary, we present a tethered soft wall-climbing robot that integrates a dielectric-elastomer actuator for fast periodic deformation of the robotic body and two electroadhesive feet for controlled adhesion of the robot on walls. The soft robot features capabilities of simple control (with only voltages), climbing on various vertical walls (made of wood, paper, and glass), carrying a payload (i.e., a camera for video recording), multimodal locomotion (climbing, crawling, and turning), and adaptive deformation (through confined spaces).

One benefit of the dielectric-elastomer actuator is allowing a robot design with simple mechanism and high flexibility. Our results show that a single dielectric-elastomer actuator provided continuum locomotion of the soft robot (*54*), which is different from traditional rigid robots that require separated actuation and transmission components. The dielectric-elastomer actuator also enables mechanically compliant interactions of the robot with environments, even squeezing its body to pass through a confined space. Although a soft crawling robot using the dielectric-elastomer actuator was recently reported (*35*), it was unable to climb walls and achieve spot turning.

The electroadhesion forces of the robot's feet (Fig. 2B) rely on not only the applied voltages but also the materials and surface textures of various substrates (fig. S9). Under the same applied voltage, the glass substrate with the smoothest surface provides the lowest electroadhesion forces among all substrates. Because the tangential electroadhesion force is used to overcome the gravity force of the robot during climbing, our robot demonstrates a lower climbing speed on the glass substrate than on other substrates (Fig. 4A). On the other hand, when crawling on horizontal planes without the challenge of gravity, the crawling speeds of the robot on various substrates under the same conditions are similar to each other (Fig. 5C). In addition, because of the active electroadhesion of our robot's feet controlled by applied voltages, our robot achieves reciprocated crawling on the plane (movie S8 and table S1), which is usually difficult for other soft crawling robots with passive adhesion mechanisms (such as adding hooks or changing the contact material stiffness) (*54*).

Although untethered robots are usually more desirable in applications, recently developed soft robots for crawling, grabbing objects, camouflaging, swimming, and growing are generally tethered (see table S1) (*36*–*44*). Currently, it is still challenging to develop untethered soft robots (*29*–*31*). We focused on creating a soft wall-climbing robot that combines the dielectric-elastomer actuator and electroadhesive feet and controlled our robot with external electrical wires to apply voltages. In future work, we will explore and integrate small high-voltage drivers and microcontrollers (*35*, *55*) into the soft robot for untethered control and operation.

MATERIALS AND METHODS

Objectives of the study

Our objective was to design a soft wall-climbing robot based on muscle-like actuators. To achieve this objective, we created a tethered soft wall-climbing robot by using a dielectric-elastomer actuator and

electroadhesive feet. We chose the dielectric-elastomer actuator as the muscle and electroadhesion for the feet such that all components of designed soft robot could be electrically controlled.

Materials and fabrication

The materials for fabricating the dielectric-elastomer actuator were made of the following commercial products: dielectric elastomers (VHB 4910 and 4905, 3M company) and carbon grease (846-80G, MG Chemical). The fabrication process (fig. S2) could be described as follows. (i) A custom-built stretcher was adopted to prestretch the dielectric-elastomer membrane. The prestretched ratio could be controlled by four fixtures (fig. S2A). (ii) A stiff acrylic frame (thickness, 5 mm) fabricated by a laser cut machine (LCF150QC1, HGTECH) was used to take the prestretched dielectric-elastomer membrane down from the stretcher and support the membrane (fig. S2B). Because of the viscoelasticity of the membrane, we kept it for about 12 hours before using it as the muscle. (iii) The side of the frame that contained stiffeners (fig. S1) was stacked to the dielectric-elastomer membrane (fig. S2C). (iv) A paintbrush coated the electrodes (carbon grease) on both sides of the membrane (fig. S2D). To avoid the electrical breakdown on the edge of the membrane, we inserted an interval of 1 mm between the electrodes and the edge of the frame. (v) After relaxing the prestretch of the membrane, the saddle-shaped dielectric-elastomer actuator formed, and two soft wires were used to connect the electrodes with a high-voltage amplifier (fig. S2E).

Description of the control platform

For controlling of the soft wall-climbing robot, we adopted the high-voltage amplifiers to drive the dielectric-elastomer actuator and electroadhesive feet, respectively. A dSPACE-DS1103 control board equipped with 16-bit analog-to-digital converters and 16-bit digital-to-analog converters was used to generate the real-time actuation signal for high-voltage amplifiers. When driving soft robots, the dielectric-elastomer actuator and electroadhesive feet were connected to an individual amplifier and independently actuated. When driving the four-foot soft robot, two dielectric-elastomer actuators shared one amplifier, and the four electroadhesive feet were divided into two groups such that each group shared one amplifier. Therefore, we used several electrical relays to program the combination, whereas all the control sequences were generated by the dSPACE-DS1103 control board.

Characterization method of electroadhesion forces

The electroadhesive foot was placed on different substrates. A soft thread was used to connect the electroadhesive foot to a three-dimensional force sensor, which was installed on a linear hail (fig. S5). To measure the normal electroadhesion force, we followed three steps: (i) At $t = 0$ s, a step voltage was applied; (ii) after 2 s, a normal movement with a constant speed of 1 mm/s was generated by the linear rail, and the force sensor recorded the tensile force of the thread, which was then analyzed as the normal electroadhesion force; and (iii) when the displacement reached 5 mm, the measurement stopped. The tangential electroadhesion force was measured by the same approach, and the only difference was that the linear hail needed to provide the tangential movement.

Characterization method of the dielectric-elastomer actuator

Blocking force

We put the soft robot on a horizontal plane. We fixed one foot and clamped the other foot on a three-dimensional force sensor that was installed on a linear rail (fig. S6). The measured steps could be described as follows: (i) The dielectric-elastomer actuator was in rest state at $t = 0$ s, and step voltage was then applied to the actuator; (ii) after 2 s, the linear rail generated a horizontal movement with a constant speed of 1 mm/s, and a three-dimensional force sensor was used to capture the blocking force; and (iii) when the displacement reached 10 mm, the measuring process stopped.

Maximum extension length

We put the soft robot on a horizontal plane (fig. S7). We drove the dielectric-elastomer actuator by sinusoidal voltage with different amplitudes and frequencies. We kept one foot fixed and measured the position of the other movable one. The position was recorded by a laser sensor. Then, the maximum extension length could be calculated on the basis of the recoded data (see fig. S8).

Data acquisition and processing

We adopted the dSPACE-DS1103 control board equipped with 16-bit analog-to-digital converters and 16-bit digital-to-analog converters to monitor the elelctroadhesive force, blocking force, and extension length. The experimental data were captured by the interface dSPACE-ControlDesk 5.2. The sampling time was set to be 1 ms for each measurement. We used MATLAB for the following data processing and plotting.

SUPPLEMENTARY MATERIALS

robotics.sciencemag.org/cgi/content/full/3/25/eaat2874/DC1
Description of the model simulation of the dielectric-elastomer actuator
Fig. S1. The structure design of the soft wall-climbing robot.
Fig. S2. The fabrication process of the dielectric-elastomer actuator.
Fig. S3. The assembly of the soft wall-climbing robot.
Fig. S4. Model simulation of the dielectric-elastomer actuator.
Fig. S5. Experimental setup for the electroadhesion measurement.
Fig. S6. Experimental setup for the blocking force measurement.
Fig. S7. Experimental setup for the extension measurement.
Fig. S8. Maximum extension length calculated in one actuation cycle.
Fig. S9. The surface topography of different substrates.
Table S1. The currently available soft crawling robots and soft climbing robots.
Movie S1. Climbing experiments without payload.
Movie S2. Climbing experiments with a 10-g payload.
Movie S3. Crawling experiments.
Movie S4. Turning experiments.
Movie S5. Video recording while climbing a vertical tunnel.
Movie S6. Confined space navigation experiment.
Movie S7. Labyrinth trajectory tracking experiment.
Movie S8. Reciprocated crawl on the glass plane.
References (*56*–*61*)

REFERENCES AND NOTES

1. K. Autumn, Y. A. Liang, S. T. Hsieh, W. Zesch, W. P. Chan, T. W. Kenny, R. Fearing, R. J. Full, Adhesive force of a single gecko foot-hair. *Nature* **405**, 681–685 (2000).
2. A. J. Ijspeert, Biorobotics: Using robots to emulate and investigate agile locomotion. *Science* **346**, 196–203 (2014).
3. H. Jiang, E. W. Hawkes, C. Fuller, M. A. Estrada, S. A. Suresh, N. Abcouwer, A. K. Han, S. Wang, C. J. Ploch, A. Parness, M. R. Cutkosky, A robotic device using gecko-inspired adhesives can grasp and manipulate large objects in microgravity. *Sci. Robot.* **2**, eaan4545 (2017).
4. S. Kim, M. Spenko, S. Trujillo, B. Heyneman, D. Santos, M. R. Cutkosky, Smooth vertical surface climbing with directional adhesion. *IEEE Trans. Robot.* **24**, 65–74 (2008).
5. O. Unver, M. Sitti, Tankbot: A palm-size, tank-like climbing robot using soft elastomer adhesive treads. *Int. J. Robot. Res.* **29**, 1761–1777 (2010).
6. M. P. Murphy, C. Kute, Y. Mengüç, M. Sitti, Waalbot II: Adhesion recovery and improved performance of a climbing robot using fibrillar adhesives. *Int. J. Robot. Res.* **30**, 118–133 (2011).

7. E. W. Hawkes, E. V. Eason, A. T. Asbeck, M. R. Cutkosky, The gecko's toe: Scaling directional adhesives for climbing applications. *IEEE ASME Trans. Mechatron.* **18**, 518–526 (2013).
8. G. Lee, H. Kim, K. Seo, J. Kim, H. S. Kim, MultiTrack: A multi-linked track robot with suction adhesion for climbing and transition. *Rob. Auton. Syst.* **72**, 207–216 (2015).
9. W. Wang, K. Wang, H. Zhang, Crawling gait realization of the mini-modular climbing caterpillar robot. *Prog. Nat. Sci.* **19**, 1821–1829 (2009).
10. R. Liang, M. Altaf, E. Ahmad, R. Liu, K. Wang, A low-cost, light-weight climbing robot for inspection of class curtains. *Int. J. Adv. Robot. Syst.* **11**, 106 (2014).
11. Y. Guan, H. Zhu, W. Wu, X. Zhou, L. Jiang, C. Cai, L. Zhang, H. Zhang, A modular biped wall-climbing robot with high mobility and manipulating function. *IEEE ASME Trans. Mechatron.* **18**, 1787–1798 (2013).
12. R. Chen, R. Liu, J. Chen, J. Zhang, A gecko inspired wall-climbing robot based on electrostatic adhesion mechanism, in *IEEE International Conference on Robotics and Biomimetics* (ROBIO, 2013), pp. 396–401.
13. H. Prahlad, R. Pelrine, S. Stanford, J. Marlow, R. Kornbluh, Electroadhesive robots—Wall climbing robots enabled by a novel, robust, and electrically controllable adhesion technology, in *IEEE International Conference on Robotics and Automation* (ICRA, 2008), pp. 3028—3033.
14. A. Yamamoto, T. Nakashima, T. Higuchi, Wall climbing mechanisms using electrostatic attraction generated by flexible electrodes, in *IEEE International Symposium on Micro-NanoMechatronics and Human Science* (MHS, 2007), pp. 389–394.
15. G. Lee, G. Wu, S. H. Kim, J. Klm, T. Seo, Combot: Compliant climbing robotic platform with transitioning capability and payload capacity, in *IEEE International Conference on Robotics and Automation* (ICRA, 2012), pp. 2737–2742.
16. F. Tâche, W. Fischer, G. Caprari, R. Siegwart, R. Moser, F. Mondada, Magnebike: A magnetic wheeled robot with high mobility for inspecting complex-shaped structures. *J. Field Robot.* **26**, 453–476 (2009).
17. G. Lee, K. Seo, S. Lee, J. Park, H. Kim, J. Kim, T. Seo, Compliant track-wheeled climbing robot with transitioning ability and high-payload capacity, in *IEEE International Conference on Robotics and Biomimetics* (ROBIO, 2011), pp. 2020–2024.
18. M. J. Spenko, G. C. Haynes, J. A. Saunders, A. A. Rizzi, R. J. Full, D. E. Koditschek, Biologically inspired climbing with a hexapedal robot. *J. Field Robot.* **25**, 223–242 (2008).
19. S. Kim, A. T. Asbeck, M. R. Cutkosky, W. R. Provancher, SpinybotII: Climbing hard walls with compliant microspines, in *International Conference on Advanced Robotics* (ICAR, 2015), pp. 601–606.
20. F. Xu, X. Wang, G. Jiang, Design and analysis of a wall-climbing robot based on a mechanism utilizing hook-like claws. *Int. J. Adv. Robot. Syst.* **9**, 261 (2012).
21. T. L. Lam, Y. A. Xu, A flexible tree climbing robot: Treebot-design and implementation, in *IEEE International Conference on Robotics and Automation* (ICRA, 2011), pp. 5849–5854.
22. Y. Liu, X. Wu, H. Qian, D. Zheng, J. Sun, Y. Xu, System and design of clothbot: A robot for flexible clothes climbing, in *IEEE International Conference on Robotics and Automation* (ICRA, 2012), pp. 1200–1205.
23. S. Kalouche, N. Wiltsie, H.-J. Su, A. Parness, Inchworm style gecko adhesive climbing robot, in *IEEE/RSJ International Conference on Intelligent Robots and Systems* (IROS, 2014), pp. 2319–2324.
24. O. Unver, M. Sitti, Flat dry elastomer adhesives as attachment materials for climbing robots. *IEEE Trans. Robot.* **26**, 131–141 (2010).
25. T. W. Seo, M. Sitti, Tank-like module-based climbing robot using passive compliant joints. *IEEE/ASME Trans. Mechatron.* **18**, 397–408 (2013).
26. J. Krahn, Y. Liu, A. Sadeghi, C. Menon, A tailless timing belt climbing platform utilizing dry adhesives with mushroom caps. *Smart Mater. Struct.* **20**, 115021 (2011).
27. H. Wang, A. Yamamoto, T. Higuchi, A crawler climbing robot integrating electroadhesion and electrostatic actuation. *Int. J. Adv. Robot. Syst.* **11**, 191 (2014).
28. H. Wang, A. Yamamoto, A thin electroadhesive inchworm climbing robot driven by an electrostatic film actuator for inspection in a narrow gap, in *IEEE International Symposium on Safety, Security, and Rescue Robotics* (SSRR, 2013), pp. 1–6.
29. C. Majidi, Soft robotics: A perspective—Current trends and prospects for the future. *Soft Robot.* **1**, 5–11 (2014).
30. D. Rus, M. T. Tolley, Design, fabrication and control of soft robots. *Nature* **521**, 467–475 (2015).
31. C. Laschi, B. Mazzolai, M. Cianchetti, Soft robotics: Technologies and systems pushing the boundaries of robot abilities. *Sci. Robot.* **1**, eaah3690 (2016).
32. C. Wang, K. Sim, J. Chen, H. Kim, Z. Rao, Y. Li, W. Chen, J. Song, R. Verduzco, C. Yu, Soft ultrathin electronics innervated adaptive fully soft robots. *Adv. Mater.* **30**, 1706695 (2018).
33. T. Umedachi, V. Vikas, B. A. Trimmer, Softworms: The design and control of non-pneumatic, 3D-printed, deformable robots. *Bioinspir. Biomim.* **11**, 025001 (2016).
34. A. Rafsanjani, Y. Zhang, B. Liu, S. M. Rubinstein, K. Bertold, Kirigami skins make a simple soft actuator crawl. *Sci. Robot.* **3**, eaar7555 (2018).
35. J. Cao, L. Qin, J. Liu, Q. Ren, C. C. Foo, H. Wang, H. P. Lee, J. Zhu, Untethered soft robot capable of stable locomotion using soft electrostatic actuators. *Extreme Mech. Lett.* **21**, 9–16 (2018).
36. J. Shintake, S. Rosset, B. Schubert, D. Floreano, H. Shea, Versatile soft grippers with intrinsic electroadhesion based on multifunctional polymer actuators. *Adv. Mater.* **28**, 231–238 (2016).
37. N. Kellaris, V. G. Venkata, G. M. Smith, S. K. Mitchell, C. Keplinger, Peano-HASEL actuators: Muscle-mimetic, electrohydraulic transducers that linearly contract on activation. *Sci. Robot.* **3**, eaar3276 (2018).
38. H. Yuk, T. Zhang, G. A. Parada, X. Liu, X. Zhao, Skin-inspired hydrogel–elastomer hybrids with robust interfaces and functional microstructures. *Nat. Commun.* **7**, 12028 (2016).
39. J. H. Pikul, S. Li, H. Bai, R. T. Hanlon, I. Cohen, R. F. Shepherd, Stretchable surfaces with programmable 3D texture morphing for synthetic camouflaging skins. *Science* **358**, 210–214 (2017).
40. C. Christianson, N. N. Goldberg, D. D. Deheyn, S. Cai, M. T. Tolley, Translucent soft robots driven by frameless fluid electrode dielectric elastomer actuators. *Sci. Robot.* **3**, eaat1893 (2018).
41. Y. Wang, X. Yang, Y. Chen, D. K. Wainwright, C. P. Kenaley, Z. Gong, Z. Liu, H. Liu, J. Guan, T. Wang, J. C. Weaver, R. J. Wood, L. Wen, A biorobotic adhesive disc for underwater hitchhiking inspired by the remora suckerfish. *Sci. Robot.* **2**, eaan8072 (2017).
42. T. Li, G. Li, Y. Liang, T. Cheng, J. Dai, X. Yang, B. Liu, Z. Zeng, Z. Huang, Y. Luo, T. Xie, W. Yang, Fast-moving soft electronic fish. *Sci. Adv.* **3**, e1602045 (2017).
43. E. W. Hawkes, L. H. Blumenschein, J. D. Greer, A. M. Okamura, A soft robot that navigates its environment through growth. *Sci. Robot.* **2**, eaan3028 (2017).
44. M. S. Verma, A. Ainla, D. Yang, D. Harburg, G. M. Whitesides, A soft tube-climbing robot. *Soft Robot.* **5**, 133–137 (2018).
45. G. Kofod, W. Wirges, M. Paajanen, S. Bauer, Energy minimization for self-organized structure formation and actuation. *Appl. Phys. Lett.* **90**, 081916 (2007).
46. R. Pelrine, R. Kornbluh, Q. Pei, J. Joseph, High-speed electrically actuated elastomers with strain greater than 100%. *Science* **287**, 836–839 (2000).
47. I. A. Anderson, T. A. Gisby, T. G. McKay, B. M. O'Brien, E. P. Calius, Multi-functional dielectric elastomer artificial muscles for soft and smart machines. *J. Appl. Phys.* **112**, 041101 (2012).
48. G. Gu, J. Zhu, L. Zhu, X. Zhu, A survey on dielectric elastomer actuators for soft robots. *Bioinspir. Biomim.* **12**, 011003 (2017).
49. M. A. Graule, P. Chirarattananon, S. B. Fuller, N. T. Jafferis, K. Y. Ma, M. Spenko, R. Kornbluh, R. J. Wood, Perching and takeoff of a robotic insect on overhangs using switchable electrostatic adhesion. *Science* **352**, 978–982 (2016).
50. D. Ruffatto III, A. Parness, M. Spenko, Improving controllable adhesion on both rough and smooth surfaces with a hybrid electrostatic/gecko-like adhesive. *J. R. Soc. Interface* **11**, 20131089 (2014).
51. A. S. Chen, S. Bergbreiter, A comparison of critical shear force in low-voltage, all-polymer electroadhesives to a basic friction model. *Smart Mater. Struct.* **26**, 025028 (2017).
52. J. Guo, T. Bamber, Y. Zhao, M. Chamberlain, L. Justham, M. Jackson, Toward adaptive and intelligent electroadhesives for robotic material handling. *IEEE Robot. Autom. Lett.* **2**, 538–545 (2017).
53. J. U. Jeon, T. Higuchi, Electrostatic suspension of dielectrics. *IEEE Trans. Ind. Electron.* **45**, 938–946 (1998).
54. M. Calisti, G. Picardi, C. Laschi, Fundamentals of soft robot locomotion. *J. R. Soc. Interface* **14**, 20170101 (2017).
55. S. I. Rich, R. J. Wood, C. Majidi, Untethered soft robotics. *Nat. Electron.* **1**, 102–112 (2018).
56. R. F. Shepherd, F. Ilievski, W. Choi, S. A. Morin, A. A. Stokes, A. D. Mazzeo, X. Chen, M. Wang, G. M. Whitesides, Multigait soft robot. *Proc. Natl. Acad. Sci. U.S.A.* **108**, 20400–20403 (2011).
57. D. Drotman, S. Jadhav, M. Karimi, P. deZonia, M. T. Tolley, 3D printed soft actuators for a legged robot capable of navigating unstructured terrain, in *Proceedings of IEEE International Conference on Robotics and Automation* (ICRA, 2017), pp. 5532–5538.
58. W. Wang, J. Y. Lee, H. Rodrigue, S. H. Song, W. S. Chu, S. H. Ahn, Locomotion of inchworm-inspired robot made of smart soft composite (SSC). *Bioinspir. Biomim.* **9**, 046006 (2014).
59. Q. Pei, R. Pelrine, S. Stanford, R. D. Kornbluh, M. S. Rosenthal, K. Meijer, R. J. Full, Multifunctional electroelastomer rolls and their application for biomimetic walking robots. *Proc. SPIE* **4698**, 246–253 (2002).
60. M. Duduta, D. R. Clarke, R. J. Wood, A high speed soft robot based on dielectric-elastomer actuators, in *Proceedings of IEEE International Conference on Robotics and Automation* (ICRA, 2017), pp. 4346–4351.
61. L. Qin, J. Cao, Y. Tang, J. Zhu, Soft freestanding planar artificial muscle based on dielectric-elastomer actuator. *J. Appl. Mech.* **85**, 051001 (2018).

Acknowledgments: Funding: This work was partially supported by the National Natural Science Foundation of China (grant nos. 51622506 and 91848204) and the Science and Technology Commission of Shanghai Municipality (grant no. 16JC1401000). **Author**

contributions: G.G. conceived the idea and designed the research. J.Z. carried out the experiments. R.Z. and X. Zhao performed the model simulation of the dielectric-elastomer actuator. G.G., J.Z., X. Zhao, and X. Zhu. analyzed and interpreted the results. G.G., X. Zhao, and X. Zhu directed the project. G.G., J.Z., X. Zhao, and X. Zhu contributed to the writing and editing of the manuscript. **Competing interests:** The authors declare that they have no competing interests. **Data and materials availability:** All data are provided in the manuscript and the Supplementary Materials.

Submitted 29 May 2018
Accepted 24 November 2018
Published 19 December 2018
10.1126/scirobotics.aat2874

Citation: G. Gu, J. Zou, R. Zhao, X. Zhao, X. Zhu, Soft wall-climbing robots. *Sci. Robot.* **3**, eaat2874 (2018).

Soft wall-climbing robots

Guoying Gu, Jiang Zou, Ruike Zhao, Xuanhe Zhao and Xiangyang Zhu

Sci. Robotics **3**, eaat2874.
DOI: 10.1126/scirobotics.aat2874